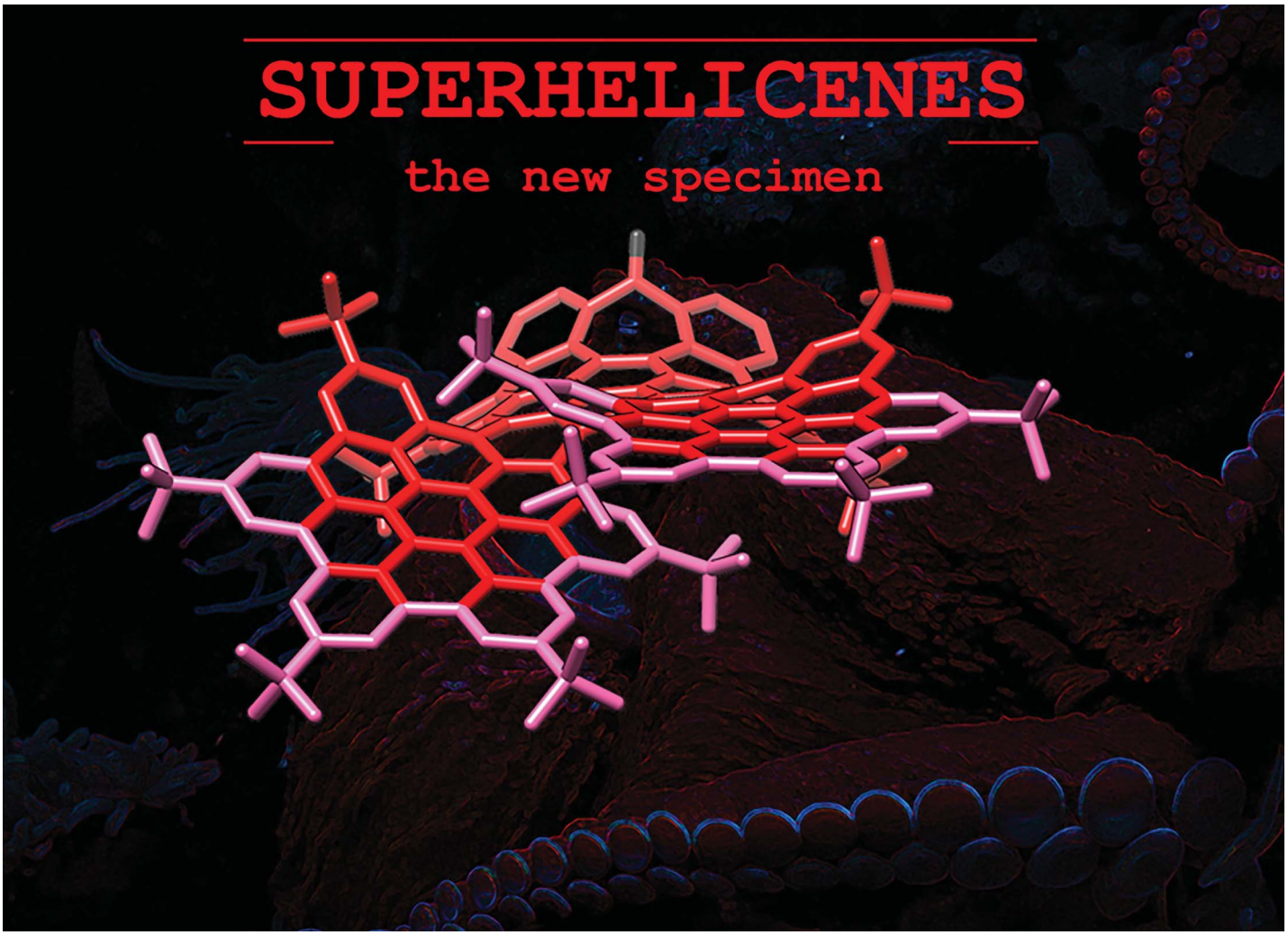

Showcasing research from Professor Campaña's laboratory, Department of Chemistry, Faculty of Sciences, University of Granada, Granada, Spain.

Highly contorted superhelicene hits near-infrared circularly polarized luminescence

A new superhelicene structure exhibits Near Infrared Circularly Polarized Luminescene (NIR-CPL) both in solution and thin films, together with upconversion-based Two Photon Absorption (TPA-UC). The emission is shifted to the NIR due to the combination of helicenes and a tropone unit.

We acknowledge @sigmund from Unsplash for the picture used in the artwork.

As featured in:

See Ermelinda Maçôas, Carlos M. Cruz, Araceli G. Campaña *et al.*, *Chem. Sci.*, 2022, **13**, 10267.

ROYAL SOCIETY OF CHEMISTRY

rsc.li/chemical-science

Registered charity number: 207890

Chemical Science

ROYAL SOCIETY OF CHEMISTRY

EDGE ARTICLE

View Article Online
View Journal | View Issue

Cite this: *Chem. Sci.*, 2022, **13**, 10267

All publication charges for this article have been paid for by the Royal Society of Chemistry

Received 20th June 2022
Accepted 19th July 2022

DOI: 10.1039/d2sc03452b

rsc.li/chemical-science

Highly contorted superhelicene hits near-infrared circularly polarized luminescence†

Sandra Míguez-Lago, [a] Inês F. A. Mariz,[b] Miguel A. Medel,[a] Juan M. Cuerva, [a] Ermelinda Maçôas, *[b] Carlos M. Cruz *[ac] and Araceli G. Campaña *[a]

Herein we describe a novel superhelicene structure consisting of three hexa-*peri*-hexabenzocoronene (HBC) units arranged in a helical geometry and creating two carbo[5]helicenes and a carbo[7]helicene. The central HBC bears a tropone moiety, which induces a saddle-helix hybrid geometry into the 3D structure of the prepared nanographene. The introduction of multiple helicenes and the position of the tropone unit trigger near-infrared circularly polarized luminescence (NIR-CPL, up to 850 nm, $|g_{lum}| = 3.0 \times 10^{-3}$) combined with good photoluminescence quantum yields ($\phi_F = 0.43$) and upconverted emission based on two-photon absorption (TPA). Compared to previously reported superhelicenes of similar size, higher quantum yields, CPL brightness, and red-shifted absorption and emission spectra are achieved. Besides, chiroptical properties of enantiopure thin films were evaluated. These findings place this novel superhelicene as the first NIR-CPL superhelicene ever reported and make it a promising candidate for use as a chiral luminescent material in optoelectronic devices.

Introduction

Carbohelicenes are chiral motifs arising from the helical arrangement of *ortho*-fused benzenoid rings.[1–4] These chiral systems have been widely studied over decades due to their appealing structures and the optical and chiroptical properties resulting from them.[5] Nevertheless, single non-functionalized helicenes lack important features for their use as near-infrared (NIR) chiral luminescent materials in optoelectronic devices, such as red shifted absorbance and fluorescence, or high photoluminescence quantum yields.[6–10] Heteroatom-doped[11] or functionalized[12–15] helicenes have been extensively investigated as an alternative to improve such properties. Remarkably, the implementation of helicenes as a component in chiral emissive electroluminescent organic semiconductors has been successfully proved.[14,16–18] So far, only one helicene-based polymer with NIR-CPL properties has been reported,[19] whereas most of the NIR-CPL emitters are based on lanthanide or transition metal-based complexes,[20–26] which often show low quantum yields or stability issues. Purely organic compounds can be used to circumvent these drawbacks; however NIR-CPL, emitters based on organic molecules are still scarce.[27–34]

Recently, the linkage of more than one carbohelicene into a single π-system in an appropriate fashion has been highlighted as a strategy to improve the limited properties of single carbohelicenes.[35,36] Thus, the fusion of carbohelicenes into different topologies allows us to design and tune the resulting optical and chiroptical properties of multiple-helicene-containing compounds.[37] Higher chiroptical responses are expected if the arrangement of the different helicenes improves the angle between the electric and magnetic transition dipole moments, increasing the dissymmetry *g* factor. Another strategy to improve the properties of pristine helicenes involves the extension of their π-conjugated system. In this regard, the family of superhelicenes, *i.e.* HBC-based helicenes,[38] has been growing fast during the last few years, and a wide variety of members can be found in the literature.[38–44] Despite an improvement in the optical properties, with red shifted absorbance and emission spectra, the obtained fluorescence quantum yields are usually poor due to the strong π–π stacking arising from the large conjugated polycyclic surfaces. Nevertheless, it has been recently shown that the deliberate incorporation of a superhelicene into a fluorescent polymeric scaffold led to an amplification of its chiroptical response,[45] opening the door to highly-efficient chiral electroluminescent materials.

Our research group, primarily interested in the preparation and study of the optical and chiroptical properties of heptagon-containing superhelicenes,[46–49] is directing its synthesis efforts

[a]*Department of Organic Chemistry, Unidad de Excelencia de Química (UEQ), Faculty of Sciences, University of Granada, Avda. Fuente Nueva s/n, 18071 Granada, Spain. E-mail: cmorenoc@ugr.es; araceligc@ugr.es*

[b]*Centro de Química Estructural and Institute of Molecular Sciences, Instituto Superior Técnico, Universidade de Lisboa, Av. Rovisco Pais, 1, 1049-001 Lisboa, Portugal. E-mail: ermelinda.macoas@tecnico.ulisboa.pt*

[c]*Department of Chemistry, University of Zurich, Winterthurerstrasse 190, 8057 Zurich, Switzerland*

† Electronic supplementary information (ESI) available: Synthesis procedures, HPLC traces, copies of NMR spectra, optical and electrochemical properties, theoretical calculations, and thin film information. See https://doi.org/10.1039/d2sc03452b

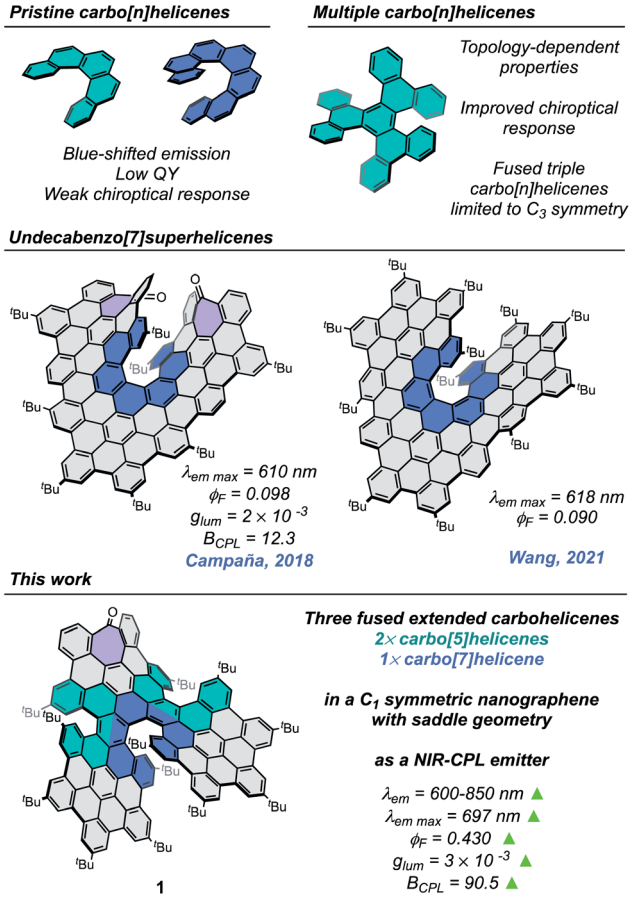

Fig. 1 Main features of pristine carbo[*n*]helicenes, multiple carbo[*n*]helicenes, and 3 × HBC-based undecabenzo[7]superhelicenes, and the structure and novel features of the herein reported compound **1**, (*M*,*M*,*P*)-**1** enantiomer are shown (chirality descriptors for [5], [7] and [5]helicene, respectively).

towards a future implementation of our HBC-based helical nanographenes in NIR chiral luminescent materials. Thus, we have designed a novel structure consisting of three HBC units, containing two extended carbo[5]helicenes, an extended carbo[7]helicene, and a seven-membered ring. The superhelicene **1** (Fig. 1) was designed to improve the low photoluminescence quantum yields of the two undecabenzo[7]superhelicenes previously reported by Wang[42] and by our research group[47] (ϕ_F = 0.090 and 0.098, respectively), and to reveal the influence of the tropone unit position and the addition of multiple carbohelicenes on the optical properties of a superhelicene scaffold.

Results and discussion

The target nanographene was obtained following the synthetic methodology developed by our research group, where the preparation and extension of heptagon-containing HBCs (*hept*-HBC) are performed by a combination of Co-catalyzed alkyne cyclotrimerization and Scholl reactions.[50] In the present case, a dibrominated diphenylacetylene partner (**3**) was required. Compound **3** was achieved under the one-pot double Sonogashira coupling conditions reported by Brisbois, Grieco and coworkers,[51] performed over 1-bromo-4-iodobenzene (**2**). The alkyne cyclotrimerization reaction between **3** and **4** afforded the heptagon-containing hexaphenylbenzene **5**, which was converted into its corresponding distorted *hept*-HBC **6** by oxidative cyclodehydrogenation. The two brominated positions in **6** were subjected to Sonogashira coupling with 4-*tert*-butylphenylacetylene, affording **7** in good yield (Scheme 1). Compound **7** was subjected to a double Diels–Alder reaction with two equivalents of 2,3,4,5-*tetrakis*-(4-*tert*-butylphenyl)-cyclopentadienone. The oligophenylene **8**, consisting of 115 carbon atoms, was subsequently placed under Scholl conditions, namely trifluoromethanesulfonic acid and 2,3-dichloro-5,6-dicyano-*p*-benzoquinone (DDQ), giving rise to **1** (Scheme 1).

The recorded ^{1}H NMR spectrum of **1** in $CDCl_3$ consisted of a mixture of isomers. Considering the configuration of the helicene moieties, three possible diastereoisomers could be formed during the last oxidative cyclodehydrogenation step, namely (*M*,*M*,*M*)-, (*M*,*M*,*P*)- and (*P*,*M*,*P*)-**1** (chirality descriptors for [5], [7] and [5]helicenes, respectively), and their corresponding enantiomers. Bearing the symmetry aspects in mind, along with tropone flipping, the configurations (*M*,*M*,*M*/*P*,*P*,*P*)-**1** and (*P*,*M*,*P*/*M*,*P*,*M*)-**1** can be regarded as C_2-symmetric structures, whilst diastereoisomer (*M*,*M*,*P*/*P*,*P*,*M*)-**1** possesses C_1 symmetry. Chiral stationary phase HPLC (CSP-HPLC) was used to perform both diastereomeric and racemic resolution simultaneously (ESI, Fig. S25†). In the chromatogram, four main peaks were found, belonging to two pairs of enantiomers after

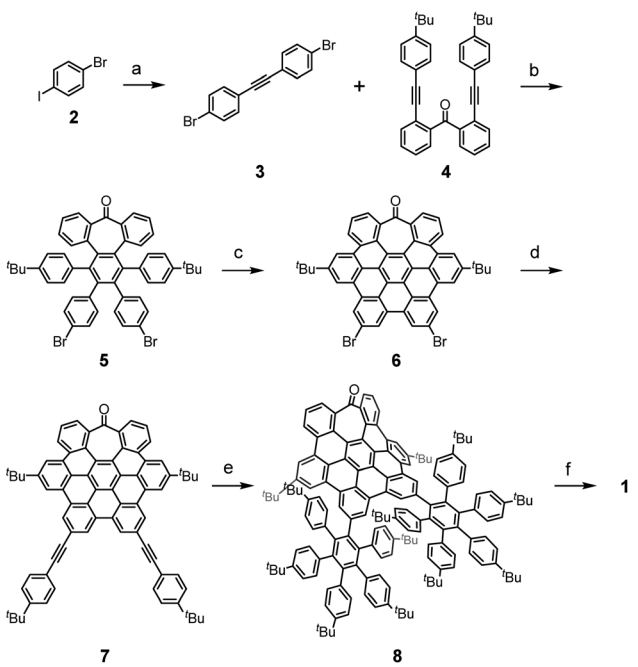

Scheme 1 Synthetic route towards the multiple-helicene-containing nanographene **1**. Reagents and conditions: (a) TMSA, $PdCl_2(PPh_3)_2$, CuI, DBU, MeCN, H_2O, 80 °C, 24 h, 84%; (b) $Co_2(CO)_8$, toluene, 110 °C, 16 h, 30%; (c) DDQ, CF_3SO_3H, CH_2Cl_2, 0 °C, 10 min, 83%; (d) 4-*tert*-butylphenylacetylene, $PdCl_2(PPh_3)_2$, CuI, Et_3N, THF, rt, 16 h, 80%; (e) 2,3,4,5-*tetrakis*-(4-*tert*-butylphenyl)-cyclopentadienone, Ph_2O, 259 °C, 64%; (f) DDQ, CF_3SO_3H, CH_2Cl_2, 0 °C, 10 min, 50%.

comparison of their UV-vis spectra. Noteworthily, when a toluene solution of **1** is refluxed for 16 h, a more understandable chromatogram is obtained, (ESI, Fig. S25†) where two chromatographic peaks with identical ^{1}H NMR spectra were found, confirming the presence of the C_1-symmetric diastereoisomer. The two chromatographic peaks belonged to the thermodynamically more stable (*M*,*M*,*P*)-**1** and (*P*,*P*,*M*)-**1** enantiomers, supporting that the interconversion barrier between the two diastereoisomers is easily surmountable at *ca.* 110 °C. Theoretical calculations (CAM-B3LYP/6-31G(d,p), gas phase) support such an interpretation, predicting the C_1-symmetric pair to be the global minimum, while the relative energy of the C_2-symmetric pairs, (*M*,*M*,*M*/*P*,*P*,*P*)-**1** and (*P*,*M*,*P*/*M*,*P*,*M*)-**1**, were calculated to be 3.32 and 10.55 kcal mol^{-1} above the global minimum, respectively. This diastereomeric distribution can be rationalized by looking at the geometries of the different diastereoisomers of compound **1**. While the saddle curvature induced by the inclusion of the seven-membered ring is well accommodated in the geometry of the pair (*M*,*M*,*P*/*P*,*P*,*M*)-**1**, for the C_2-symmetric pairs (*M*,*M*,*M*/*P*,*P*,*P*)-**1** and (*P*,*M*,*P*/*M*,*P*,*M*)-**1** the configuration of the [5]helicenes causes a partial planarization of the central *hept*-HBC unit (ESI, Fig. S32 and S34†). This fact leads to an increase in the relative energies of the C_2-symmetric diastereoisomers, supporting the interconversion towards the C_1-symmetric diastereoisomer upon heating. Moreover, suitable crystals for X-ray diffraction (XRD) were grown by slow evaporation of a CH_2Cl_2/hexane solution of (*M*,*M*,*P*/*P*,*P*,*M*)-**1** at room temperature. The quality of the crystals was low, but good enough for a preliminary structural analysis of **1**. In this sense, we found a good agreement between the main features of the structure obtained from the XRD studies and those calculated by DFT methods. From the DFT optimized structure of (*M*,*M*,*P*)-**1**, the average torsion angle (φ, Fig. 2c) of the [7]helicene moiety shows a value of 26.37°, a remarkably high value (in good agreement with the obtained XRD data, φ = 25.05°). On the other hand, the [5]helicenes show a φ = 24.82° and 25.46° according to DFT (φ = 25.35° and 26.97° according to XRD data), for the [5]helicene with the same and opposite configurations to the [7]helicene, respectively (Fig. 2d). These values are remarkably higher than those reported for pristine [5]helicene (φ = 22.10°)[52] and [7]helicene (φ = 21.97°).[53] The presence of the [7] and [5]helicene moieties, together with *hept*-HBC induces a negative curvature to one of the HBC units, exhibiting a calculated bending angle (θ, Fig. 2) of 29.11° (28.58° according to XRD). The central *hept*-HBC unit shares seven benzenoid rings with the three carbohelicenes. This fact is observed as a pronounced curvature of the *hept*-HBC unit, exhibiting an end-to-end distance (*d*, Fig. 2) of 9.41 Å (9.43 Å from XRD), remarkably lower than the one reported for pristine *hept*-HBC (10.63 Å)[50] or the *hept*-HBC sharing a carbo[5]helicene unit with HBC (10.87 Å).[46]

Compound **1** exhibited good solubility in common organic solvents, presenting a dark green color in low concentration solutions (*ca.* 10^{-6} M) that turns nearly black at a higher concentration (*ca.* 10^{-3} M). (*M*,*M*,*P*/*P*,*P*,*M*)-**1** showed a panchromatic absorption spectrum ranging from 250 to 700 nm with defined maxima centered at 365 nm (ε = 1.45 × 10^5 L mol^{-1} cm^{-1}), 505 nm (ε = 6.00 × 10^4 L mol^{-1} cm^{-1}) and a red shifted broad band extending up to 700 nm (Fig. 3a). This low-energy band is mainly dominated by a pure HOMO → LUMO transition according to TD-DFT (CAM-B3LYP/6-31G(d,p), gas phase), which was calculated at 617 nm (Fig. 3c). These red-shifted absorbance wavelengths are comparable to those measured for the green nanographene propeller reported by Wang and co-workers.[40] Upon excitation at 370 nm, an extended emission spectrum along the 600–850 nm range was obtained, with a maximum centered at 697 nm. The Stokes shift was quite low, not exceeding 50 nm. In the previous undecabenzo[7]helicenes, the HOMO and LUMO orbitals are located at the central flat HBC unit, while in (*M*,*M*,*P*/*P*,*P*,*M*)-**1** they fall all over the helicene moieties (Fig. 3c). This fact could originate through space interactions, causing red-shifted absorption and emission.[54] Furthermore, the optical HOMO–LUMO gap, taken from the crossing point between the absorbance and emission spectra, was estimated to be 1.95 eV, in perfect agreement with the measured electrochemical bandgap (1.95 eV, ESI, Fig. S31†).

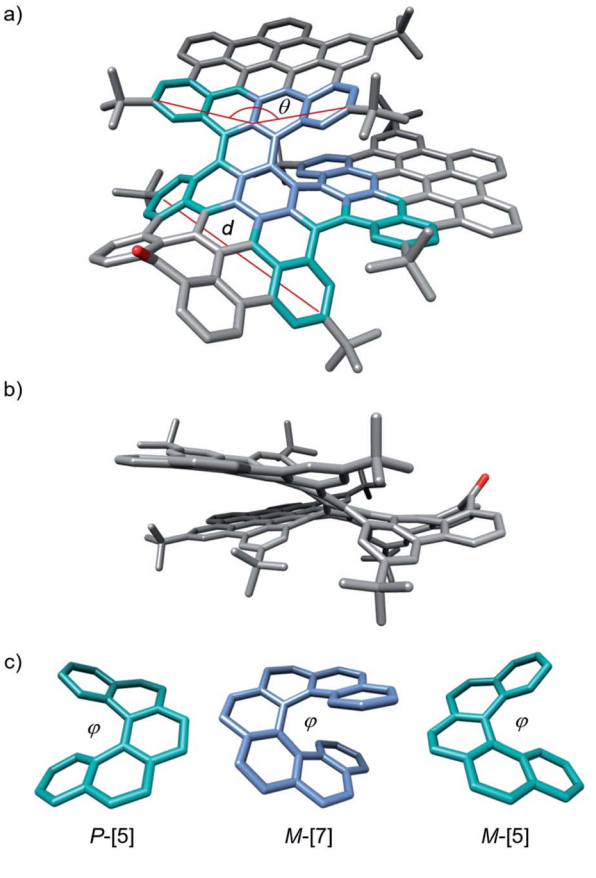

d)

Torsion angle (φ)	*P*-[5]	*M*-[7]	*M*-[5]
(*M*,*M*,*P*)-**1** - *DFT*	25.46°	26.37°	24.82°
Pristine helicenes	22.10°	21.97°	22.10°

Fig. 2 (a) DFT optimized geometry of (*M*,*M*,*P*)-**1** (CAM-B3LYP/6-31G(d,p), gas phase; lateral ^{t}Bu groups removed to reduce computational time); (b) side view; (c) [*n*]helicene structures extracted from the optimized geometry; (d) values of the measured torsion angles from the DFT optimized (*M*,*M*,*P*)-**1** and XRD structures of pristine helicenes.

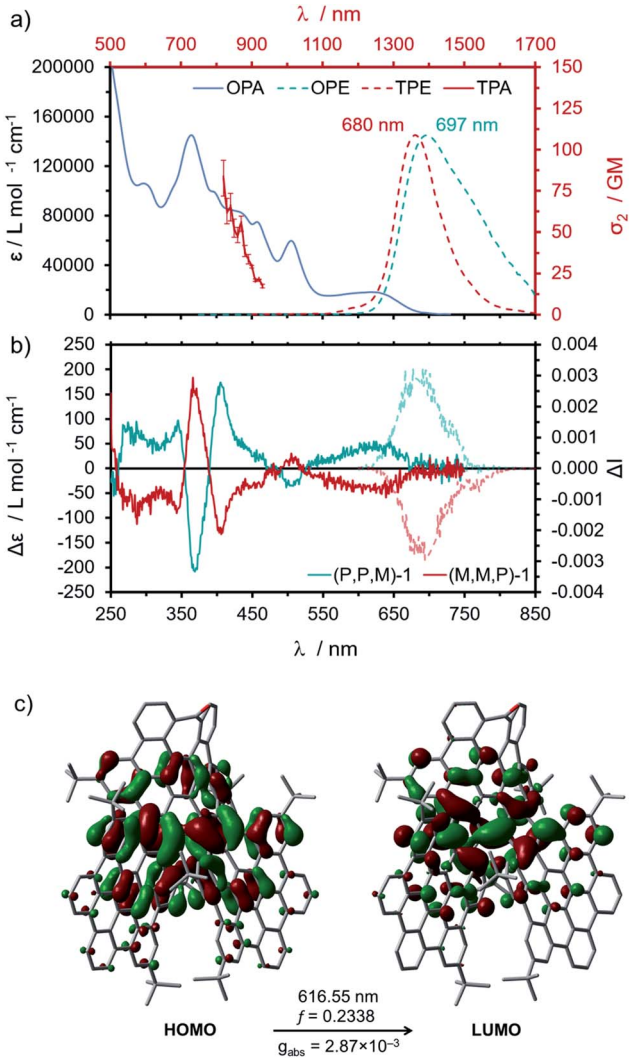

Fig. 3 (a) Experimental OPA (gray), OPE (turquoise, dashed), TPA (red) and TPE (red, dashed) spectra of (*M*,*M*,*P*/*P*,*P*,*M*)-**1**. Measured in $CHCl_3$ at *ca.* 1×10^{-6} M, $\lambda_{exc} = 370$ nm for OPE, $\lambda_{exc} = 900$ nm for TPE; (b) experimental ECD spectra of (*M*,*M*,*P*)-**1** (red) and (*P*,*P*,*M*)-**1** (turquoise) measured in $CHCl_3$ at *ca.* 1×10^{-6} M, and experimental CPL spectra ($\lambda_{exc} = 370$ nm) of (*M*,*M*,*P*)-**1** (pale red, dashed) and (*P*,*P*,*M*)-**1** (pale turquoise, dashed) measured in $CHCl_3$ at *ca.* 1×10^{-6} M; (c) HOMO and LUMO orbitals, and information of the TD-DFT calculated (CAM-B3LYP/6-31G(d,p)) lowest energy transition. The OPE spectrum is cropped at long wavelengths due to the use of a short path filter to block the multiphoton laser at the entrance of the photodetector.

The fluorescence quantum yield ($\phi_F = 0.43$ in $CHCl_3$) was estimated to be four times higher than the ones reported for the two undecabenzo-[7]superhelicenes (0.098 and 0.090),[42,47] with a monoexponential fluorescence lifetime (τ) of 6.1 ns. Similar values were obtained in dimethyl sulfoxide, a solvent of higher polarity (ESI, Table S2 and Fig. S27 and S28†). The obtained value for τ is three times lower compared to the previous undecabenzo[7]superhelicene[47] ($\tau = 18$ ns). This fact suggests that the increment in the ϕ_F is due to a faster radiative relaxation for (*M*,*M*,*P*/*P*,*P*,*M*)-**1**. Excitation with a femtosecond laser above 820 nm wavelength caused the simultaneous absorption of two NIR-photons, leading to emission at higher energies. The upconverted emission spectrum is depicted in Fig. 3a (TPE). The TPE spectrum exhibited a similar maximum when compared to its one-photon emission (Fig. 3a, OPE) spectrum, suggesting that the final relaxed excited states upon one- and two-photon excitation are the same. The log–log plot of the emission intensity as a function of excitation power showed a slope of ~2 confirming the two-photon nature of the excitation process (ESI, Fig. S29†). The two-photon absorption spectrum (Fig. 3a, TPA) showed a maximum at higher energies with TPA cross-sections of *ca.* 110 GM at 820 nm. Estimation of the TPA cross-section below 820 nm is not possible due to interference from direct one-photon absorption. In addition, the lower energy limit for the measurement of the TPA spectra is dictated by the operation range of the Ti : sapphire laser (730–900 nm).

The abovementioned CSP-HPLC racemic resolution of the pair (*M*,*M*,*P*/*P*,*P*,*M*)-**1** allowed the chiroptical property study. Thus, the ECD spectra of a chloroform solution at a concentration of 1×10^{-6} M of (*M*,*M*,*P*)- and (*P*,*P*,*M*)-**1** were recorded (Fig. 3b). Mirror-image ECD spectra were obtained for both enantiomers, with a strong bisignated signal at 390 nm, exhibiting an intense Cotton effect at 366 nm ($|\Delta\varepsilon| = 200$ L mol^{-1} cm^{-1}, $g_{abs} = 1.5 \times 10^{-3}$), and a red-shifted band that extends from 520 to 675 nm ($|\Delta\varepsilon| = 54$ L mol^{-1} cm^{-1}, $g_{abs} = 3 \times 10^{-3}$). Remarkably, the dissymmetry factor of the last band was well estimated by TD-DFT calculations ($|g_{abs}|_{calc} = 2.87 \times 10^{-3}$). The absolute configuration was assigned comparing the experimental and TD-DFT simulated ECD spectra (ESI, Fig. S39†). Thus, the first eluted peak after CSP-HPLC, with a positive Cotton effect at 600 nm, was assigned to the (*P*,*P*,*M*) enantiomer, while the second eluted peak belonged to the (*M*,*M*,*P*) enantiomer. Remarkably, both enantiomers showed a CPL response in the 600 to 800 nm range after irradiation with 370 nm wavelength, exhibiting $|g_{lum}|$ values of 3×10^{-3} (Fig. 3b), higher than that reported for the undecabenzo[7] superhelicene (2×10^{-3}).[47] In addition, the improvement of the overall efficiency of (*M*,*M*,*P*)/(*P*,*P*,*M*)-**1** is evidenced by its high CPL brightness ($B_{CPL} = \varepsilon \times \phi_F \times |g_{lum}|/2$)[55] of 90.5 L mol^{-1} cm^{-1} at λ_{exc} 365 nm, more than seven times higher than the one reported for the undecabenzo[7]superhelicene ($B_{CPL} = 12.3$ L

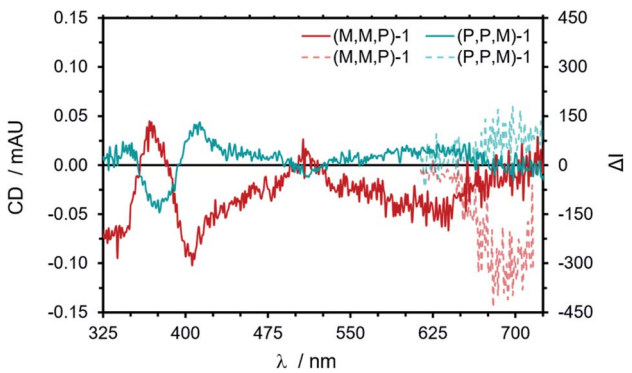

Fig. 4 Experimental ECD spectra of films of (*M*,*M*,*P*)-**1** (red) and (*P*,*P*,*M*)-**1** (turquoise) and experimental CPL spectra ($\lambda_{exc} = 370$ nm) of (*M*,*M*,*P*)-**1** (pale red, dotted) and (*P*,*P*,*M*)-**1** (pale turquoise, dotted) on quartz substrates from $CHCl_3$ solutions at *ca.* 5 mg mL^{-1}.

mol^{-1} cm^{-1}, λ_{exc} 472 nm),[47] standing out among most of the helicenes for which B_{CPL} was reported.

The OLED industry has been deeply interested in chiral emitters in the last few years.[56,57] Thin films are a common format for the implementation of these luminophores into final devices. Thus, preliminary studies using **1** were conducted to obtain thin films on quartz plates. Posterior optical and morphological examination *via* optical (OM) and tapping-mode atomic force microscopy (AFM) was carried out. Solutions of **1** in $CHCl_3$/toluene mixtures ranging from 0 to 100% toluene were tested, obtaining the best results *via* drop casting of 0.1 mg mL^{-1} solutions in pure toluene. AFM revealed wide homogeneous areas of *ca.* 100 × 100 μm constituted by stacked flakes (*ca.* 5 μm) where height profiles of *ca.* 1.6 to 2.4 nm (coincident with superhelicene dimensions) hint at the presence of stacked monolayers (ESI, Fig. S43–S46†).

Based on this initial study, enantiopure thin film formation was pursued with both (*M*,*M*,*P*)- and (*P*,*P*,*M*)-**1**. In this case, higher concentration solutions (*ca.* 5 mg mL^{-1} in $CHCl_3$) deposited *via* drop-casting led to films with observable absorptions of *ca.* 0.25 au. (ESI, Fig. S47†). Both absorption and emission spectra perfectly reproduced the band patterns measured in solution (ESI, Fig. S48†), and the same was observed for the ECD and CPL spectra (Fig. 4). The obtained $|g_{abs}|$ and $|g_{lum}|$ reached values between 1×10^{-3} and 3×10^{-3} (ESI, Fig. S50 and S51†). To prove the absence of anisotropy effects, the CPL spectra of both enantiomers were recorded from the back side and by turning the quartz substrate by 180°, observing the same sign for each enantiomer (ESI, Fig. S52†).

Conclusions

In summary, we have designed and prepared a novel superhelicene structure consisting of a central *hept*-HBC and two HBC units connected in order to form three carbohelicene moieties. The highly distorted helical nanographene shows panchromatic absorption, extending up to 700 nm, and a higher fluorescence quantum yield compared to similar sized superhelicenes previously reported. Fluorescence can be triggered either by one or two photon absorption, as found by TPA experiments. In addition, compound **1** is a NIR-CPL emitter with g_{lum} values of 3×10^{-3} both in solution and in the solid state (thin films). The combination of the optical and chiroptical properties, makes this distorted superhelicene a great candidate for use as a near-infrared (NIR) chiral luminescent material for the development of new optoelectronic devices.[58]

Data availability

We have provided all the necessary data in the ESI file.†

Author contributions

Conceptualization: E. M., C. M. C., and A. G. C.; funding acquisition: A. G. C. and E. M.; formal analysis: S. M. L., I. F. A. M., C. M. C., and J. M. C.; investigation: S. M. L., I. F. A. M., C. M. C., and M. A. M.; methodology: S. M. L., I. F. A. M., M. A. M., and C. M. C.; supervision: J. M. C., C. M. C., E. M., and A. G. C.; project administration: C. M. C., A. G. C., and E. M.; writing-original draft: C. M. C. and S. M. L.; writing-review and editing: S. M. L., J. M. C., E. M., C. M. C., and A. G. C.

Conflicts of interest

There are no conflicts to declare.

Acknowledgements

We acknowledge the European Research Council (ERC) under the European Union's Horizon 2020 research and innovation program (Grand Agreement 677023), project PGC2018-101181-B-I00 funded by MCIN/AEI/10.13039/501100011033 FEDER "Una manera de hacer Europa" and Ministerio de Economía y Competitividad (BES-2016-076371). EM acknowledges funding from Fundação para a Ciência e a Tecnologiags4: (UIDB/00100/2020, LA/P/0056/2020, PTDC/NAN-MAT/29317/2017 and 2020.01763.CEECIND). SML acknowledges the Spanish Junta de Andalucía for the funding. The authors thank the Centro de Servicios de Informática y Redes de Comunicación (CSIRC), Universidad de Granada, for providing the computing time.

Notes and references

1 R. H. Martin, *Angew. Chem., Int. Ed.*, 1974, **13**, 649–660.
2 M. Gingras, *Chem. Soc. Rev.*, 2013, **42**, 968–1006.
3 M. Gingras, G. Félix and R. Peresutti, *Chem. Soc. Rev.*, 2013, **42**, 1007–1050.
4 M. Gingras, *Chem. Soc. Rev.*, 2013, **42**, 1051–1095.
5 F. Furche, R. Ahlrichs, C. Wachsmann, E. Weber, A. Sobanski, F. Vogtle and S. Grimme, *J. Am. Chem. Soc.*, 2000, **122**, 1717–1724.
6 E. Vander Donckt, J. Nasielski, J. R. Greenleaf and J. B. Birks, *Chem. Phys. Lett.*, 1968, **2**, 409–410.
7 J. B. Birks, D. J. S. Birch, E. Cordemans and E. Vander Donckt, *Chem. Phys. Lett.*, 1976, **43**, 33–36.
8 H. Zheng, W. Li, W. Li, X. Wang, Z. Tang, S. X. A. Zhang and Y. Xu, *Adv. Mater.*, 2018, **30**, 1–7.
9 W. Zhao, W. Zhang, R. Y. Wang, Y. Ji, X. Wu and X. Zhang, *Adv. Funct. Mater.*, 2019, **29**, 1–10.
10 X. Jin, Y. Sang, Y. Shi, Y. Li, X. Zhu, P. Duan and M. Liu, *ACS Nano*, 2019, **13**, 2804–2811.
11 K. Dhbaibi, L. Favereau and J. Crassous, *Chem. Rev.*, 2019, **119**, 8846–8953.
12 W.-L. Zhao, M. Li, H.-Y. Lu and C.-F. Chen, *Chem. Commun.*, 2019, **55**, 13793–13803.
13 H. Kubo, T. Hirose, T. Nakashima, T. Kawai, J. Hasegawa and K. Matsuda, *J. Phys. Chem. Lett.*, 2021, **12**, 686–695.
14 K. Dhbaibi, L. Abella, S. Meunier-Della-Gatta, T. Roisnel, N. Vanthuyne, B. Jamoussi, G. Pieters, B. Racine, E. Quesnel, J. Autschbach, J. Crassous and L. Favereau, *Chem. Sci.*, 2021, **12**, 5522–5533.
15 D. Göbel, S. Míguez-Lago, M. J. Ruedas-Rama, A. Orte, A. G. Campaña and M. Juríček, *Helv. Chim. Acta*, 2022, **105**, e202100221.

16 Y. Yang, R. C. da Costa, D. Smilgies, A. J. Campbell and M. J. Fuchter, *Adv. Mater.*, 2013, **25**, 2624–2628.
17 L. Wan, J. Wade, X. Shi, S. Xu, M. J. Fuchter and A. J. Campbell, *ACS Appl. Mater. Interfaces*, 2020, **12**, 39471–39478.
18 L. Wan, X. Shi, J. Wade, A. J. Campbell and M. J. Fuchter, *Adv. Opt. Mater.*, 2021, 2100066.
19 K. Dhbaibi, C. Shen, M. Jean, N. Vanthuyne, T. Roisnel, M. Górecki, B. Jamoussi, L. Favereau and J. Crassous, *Front. Chem.*, 2020, **8**, 237.
20 C. L. Maupin, R. S. Dickins, L. G. Govenlock, C. E. Mathieu, D. Parker, J. A. Gareth Williams and J. P. Riehl, *J. Phys. Chem. A*, 2000, **104**, 6709–6717.
21 J.-R. Jiménez, B. Doistau, C. M. Cruz, C. Besnard, J. M. Cuerva, A. G. Campaña and C. Piguet, *J. Am. Chem. Soc.*, 2019, **141**, 13244–13252.
22 C. Dee, F. Zinna, W. R. Kitzmann, G. Pescitelli, K. Heinze, L. Di Bari and M. Seitz, *Chem. Commun.*, 2019, **55**, 13078–13081.
23 F. Zinna, L. Arrico and L. Di Bari, *Chem. Commun.*, 2019, **55**, 6607–6609.
24 B. Lefeuvre, C. A. Mattei, J. F. Gonzalez, F. Gendron, V. Dorcet, F. Riobé, C. Lalli, B. Le Guennic, O. Cador, O. Maury, S. Guy, A. Bensalah-Ledoux, B. Baguenard and F. Pointillart, *Chem.–Eur. J.*, 2021, **27**, 7362–7366.
25 J. Jiménez, M. Poncet, S. Míguez-Lago, S. Grass, J. Lacour, C. Besnard, J. M. Cuerva, A. G. Campaña and C. Piguet, *Angew. Chem., Int. Ed.*, 2021, **60**, 10095–10102.
26 N. F. M. Mukthar, N. D. Schley and G. Ung, *J. Am. Chem. Soc.*, 2022, **144**, 6148–6153.
27 K. Miki, T. Noda, M. Gon, K. Tanaka, Y. Chujo, Y. Mizuhata, N. Tokitoh and K. Ohe, *Chemistry*, 2019, **25**, 9211–9216.
28 C. Maeda, K. Suka, K. Nagahata, K. Takaishi and T. Ema, *Chem.–Eur. J.*, 2020, **26**, 4261–4268.
29 J. Feng, L. Fu, H. Geng, W. Jiang and Z. Wang, *Chem. Commun.*, 2020, **56**, 912–915.
30 T. Gao, Z. Jiang, B. Chen, Q. Sun, Y. Orooji, L. Huang and Z. Liu, *Dyes Pigm.*, 2020, **173**, 107998.
31 J. Jiménez, F. Moreno, B. L. Maroto, T. A. Cabreros, A. S. Huy, G. Muller, J. Bañuelos and S. de la Moya, *Chem. Commun.*, 2019, **55**, 1631–1634.
32 S. H. Pun, K. M. Cheung, D. Yang, H. Chen, Y. Wang, S. V. Kershaw and Q. Miao, *Angew. Chem., Int. Ed.*, 2022, **61**, e202113203.
33 Y. Nakakuki, T. Hirose and K. Matsuda, *Org. Lett.*, 2022, **24**, 648–652.
34 J. Wang, C. Shen, G. Zhang, F. Gan, Y. Ding and H. Qiu, *Angew. Chem., Int. Ed.*, 2022, **61**, e202115979.
35 C. Li, Y. Yang and Q. Miao, *Chem.–Asian J.*, 2018, **13**, 884–894.
36 T. Mori, *Chem. Rev.*, 2021, **121**, 2373–2412.
37 H. Tanaka, M. Ikenosako, Y. Kato, M. Fujiki, Y. Inoue and T. Mori, *Commun. Chem.*, 2018, **1**, 38.
38 D. Reger, P. Haines, F. W. Heinemann, D. M. Guldi and N. Jux, *Angew. Chem., Int. Ed.*, 2018, **57**, 5938–5942.
39 P. J. Evans, J. Ouyang, L. Favereau, J. Crassous, I. Fernández, J. Perles and N. Martín, *Angew. Chem., Int. Ed.*, 2018, **57**, 6774–6779.
40 Y. Zhu, X. Guo, Y. Li and J. Wang, *J. Am. Chem. Soc.*, 2019, **141**, 5511–5517.
41 J. Ma, Y. Fu, E. Dmitrieva, F. Liu, H. Komber, F. Hennersdorf, A. A. Popov, J. J. Weigand, J. Liu and X. Feng, *Angew. Chem., Int. Ed.*, 2020, **59**, 5637–5642.
42 Y. Chen, C. Lin, Z. Luo, Z. Yin, H. Shi, Y. Zhu and J. Wang, *Angew. Chem., Int. Ed.*, 2021, **60**, 7796–7801.
43 D. Reger, P. Haines, K. Y. Amsharov, J. A. Schmidt, T. Ullrich, S. Bönisch, F. Hampel, A. Görling, J. Nelson, K. E. Jelfs, D. M. Guldi and N. Jux, *Angew. Chem., Int. Ed.*, 2021, **60**, 18073–18081.
44 J. Urieta-Mora, M. Krug, W. Alex, J. Perles, I. Fernández, A. Molina-Ontoria, D. M. Guldi and N. Martín, *J. Am. Chem. Soc.*, 2020, **142**, 4162–4172.
45 J. Wade, J. R. Brandt, D. Reger, F. Zinna, K. Y. Amsharov, N. Jux, D. L. Andrews and M. J. Fuchter, *Angew. Chem., Int. Ed.*, 2021, **60**, 222–227.
46 C. M. Cruz, I. R. Márquez, I. F. A. Mariz, V. Blanco, C. Sánchez-Sánchez, J. M. Sobrado, J. A. Martín-Gago, J. M. Cuerva, E. Maçôas and A. G. Campaña, *Chem. Sci.*, 2018, **9**, 3917–3924.
47 C. M. Cruz, S. Castro-Fernández, E. Maçôas, J. M. Cuerva and A. G. Campaña, *Angew. Chem., Int. Ed.*, 2018, **57**, 14782–14786.
48 C. M. Cruz, I. R. Márquez, S. Castro-Fernández, J. M. Cuerva, E. Maçôas and A. G. Campaña, *Angew. Chem., Int. Ed.*, 2019, **58**, 8068–8072.
49 S. Castro-Fernández, C. M. Cruz, I. F. A. Mariz, I. R. Márquez, V. G. Jiménez, L. Palomino-Ruiz, J. M. Cuerva, E. Maçôas and A. G. Campaña, *Angew. Chem., Int. Ed.*, 2020, **59**, 7139–7145.
50 I. R. Márquez, N. Fuentes, C. M. Cruz, V. Puente-Muñoz, L. Sotorrios, M. L. Marcos, D. Choquesillo-Lazarte, B. Biel, L. Crovetto, E. Gómez-Bengoa, M. T. González, R. Martin, J. M. Cuerva and A. G. Campaña, *Chem. Sci.*, 2017, **8**, 1068–1074.
51 M. J. Mio, L. C. Kopel, J. B. Braun, T. L. Gadzikwa, K. L. Hull, R. G. Brisbois, C. J. Markworth and P. A. Grieco, *Org. Lett.*, 2002, **4**, 3199–3202.
52 R. Kuroda, *J. Chem. Soc., Perkin Trans. 2*, 1982, 789–794.
53 M. Joly, N. Defay, R. H. Martin, J. P. Declerq, G. Germain, B. Soubrier-Payen and M. Van Meerssche, *Helv. Chim. Acta*, 1977, **60**, 537–560.
54 J. Liu, H. Zhang, L. Hu, J. Wang, J. W. Y. Lam, L. Blancafort and B. Z. Tang, *J. Am. Chem. Soc.*, 2022, **144**, 7901–7910.
55 L. Arrico, L. Di Bari and F. Zinna, *Chem.–Eur. J.*, 2021, **27**, 2920–2934.
56 F. Song, Z. Xu, Q. Zhang, Z. Zhao, H. Zhang, W. Zhao, Z. Qiu, C. Qi, H. Zhang, H. H. Y. Sung, I. D. Williams, J. W. Y. Lam, Z. Zhao, A. Qin, D. Ma and B. Z. Tang, *Adv. Funct. Mater.*, 2018, **28**, 1800051.
57 M. Li, Y. Wang, D. Zhang, L. Duan and C. Chen, *Angew. Chem., Int. Ed.*, 2020, **59**, 3500–3504.
58 P. Stachelek, L. MacKenzie, D. Parker and R. Pal, *Nat. Commun.*, 2022, **13**, 553.